Comparing the Dynamic Global Core Plasma Model (DGCPM) With Ground-Based Plasma Mass Density Observations

Anders M. Jorgensen,[1] Balazs Heilig,[2] Massimo Vellante,[3] Janos Lichtenberger,[4,5] Jan Reda,[6] Fridrich Valach,[7] Igor Mandic[8]

Abstract. The Dynamic Global Core Plasma Model (DGCPM) is an empirical dynamical model of the plasmasphere which, despite its simple mathematical form, or perhaps because of its simple mathematical form, has enjoyed wide use in the space physics modeling community. In this paper we present some recent observations from the European quasi-Meridional Magnetometer Array (EMMA) and compare these with the DGCPM. The observations suggest more rapid daytime refilling and loss than what is described in the DGCPM. We then modify the DGCPM by changing the values of some of its parameters, leaving the functional form intact. The modified DGCPM agrees much better with the EMMA observations. The modification resulted in an order-of-magnitude faster daytime refilling and nighttime loss. These results are also consistent with previous observations of daytime refilling.

1. Introduction

The plasmasphere is now recognized as a critical component of the coupled inner magnetosphere together with the ionosphere, thermosphere, radiation belts, and ring current. Plasma density gradients, especially the plasmapause, are sites of wave activity which control the formation and decay of the radiation belts.

A number of plasmasphere models exist which seek to describe the system. We are using the Dynamic Global Core Plasma Model (DGCPM) [*Ober et al.*, 1997] which is a two-dimensional empirical model of the flux-tube content. Other models include the SAMI3 model [*Huba et al.*, 2008] (SAMI3 is a acronym for Sami3 is Also a Model of the Ionosphere) which is a fluid model of the ionosphere and plasmasphere, modeling multiple species, the Field Line Interhemispheric Plasma model (FLIP) [*Richards et al.*, 2000] which models multiple species on a single field line, the Ionosphere-Plasmasphere (IP) model [*Maruyama et al.*, 2016] which is a 3-dimensional expansion of the FLIP model, and a 3D Kinetic Model of the plasmasphere and ionosphere [*Pierrard and Stegen*, 2008].

This paper was motivated by the relatively large disagreement between the DGCPM and plasma mass density observations deduced from ground-based magne-

[1]New Mexico Institute of Mining and Technology, Socorro, NM, USA
[2]Geological and Geophysical Institute of Hungary, Budapest, Hungary
[3]University of LAquila, LAquila, Italy
[4]Eötvös University, Budapest, Hungary
[5]Geodetic and Geophysical Institute, RCAES, Hungarian Academy of Sciences, Sopron, Hungary
[6]Institute of Geophysics, Polish Academy of Sciences, Warsaw, Poland
[7]Geomagnetic Observatory, Earth Science Institute, Slovak Academy of Sciences, Hurbanovo, Slovakia
[8]Department of Geophysics, University of Zagreb, Zagreb, Croatia

Copyright 2017 by the American Geophysical Union.
0148-0227/17/$9.00

tometer observations using the field-line resonance technique. In order to obtain agreement it is necessary to invoke refilling and loss rates which are an order of magnitude faster than those used by *Ober et al.* [1997].

Before proceeding we should clarify what we mean by refilling because the same term is used in two different contexts. The plasmasphere plasma density generally decreases when its ionospheric footpoints are in darkness and increases when its ionospheric footpoints are in daylight. The increase in plasma density when the footpoint is on the dayside of the Earth is what we will call the daytime refilling, and it is the process which we are studying in this paper. The other use of the term refilling is the day-to-day refilling over the longer term after erosion of the plasmasphere density, for example in a magnetic storm. The day-to-day refilling is nothing more than the net difference between the daytime refilling and the nighttime depletion. In this paper we do not study the day-to-day refilling.

Another important point to make clear is that the DGCPM models electron density whereas the FLR observations produce mass density. In our analysis we fit the DGCPM to the mass density measurements thus producing a dynamic model of mass density instead of electron density. The majority of plasmaspheric plasma is singly-ionized, and thus the ratio of mass density in units of amu per volume to electron number density (per same volume) equals the average mass per ion in amu. *Berube et al.* [2005] obtained the average ion mass as a function of L-shell by comparing their mass density observations with IMAGE RPI electron density measurements (see their Figure 3 and references in their paper to the IMAGE RPI results). Their figure extends to L=3.1, at that point the average ion mass appears to be approximately 1.3 with an uncertainty range from 0.7 to 1.8. We read these values off the figure so they are not exact. *Takahashi et al.* [2006] obtained mass density values consistent with Berube inside the plasmasphere as well as during quieter times, and larger values for more active times and outside the plasmasphere. *Obana et al.* [2010] considered it reasonable to assume a mass ratio of 3 in order to compare their derived upward daytime mass fluxes with previous determinations of upward electron fluxes (based on the analysis by *Takahashi et al.* [2006]). However these numbers are not consistent with the mass ratios measured by *Lichtenberger et al.* [2013] which were approximately equal to unity.

A number of observations and models have been used to measure the plasmasphere refilling rate, both the day-to-day refilling and the daily refilling rate. First we present a few results for day-to-day refilling studies from the literature and then we discuss previous results for the daytime refilling.

Lawrence et al. [1999] studied the long-term, day-to-day refilling at geostationary orbit based on LANL/MPA data and found evidence for a two-stage refilling process with the early-stage refilling rate in the range 0.6-12 $\mathrm{cm}^{-3}\,\mathrm{day}^{-1}$ and the late-stage refilling rate in the range of 10-50 $\mathrm{cm}^{-3}\,\mathrm{day}^{-1}$ (see their paper for details). In a longer-term study *Su et al.* [2001] confirmed these results with early-stage refilling rate in the range 2.5 -6.5 $\mathrm{cm}^{-3}\,\mathrm{day}^{-1}$ and late-stage refilling in the range of 10-25 $\mathrm{cm}^{-3}\,\mathrm{day}^{-1}$.

Borovsky et al. [2014] studied long-lived plasma plumes and argued that the refilling rate in existing plasmaspheric models is insufficient to explain these. A much larger refilling rate is necessary in order to explain them.

They daytime refilling rate has also been studied extensively. *Chi et al.* [2000] studied the period around a geomagnetic storm using IGPP/LANL magnetometers and found the daytime refilling rate to be 200 amu cm^{-3} hr^{-1} near $L = 2$. *Obana et al.* [2010] studied refilling for three storms in 2004 and 2001 using data from magnetometers in Finland, UK, and North America. They found refilling rates of 13 amu cm^{-3} hr^{-1} at $L = 3.8$, 39 amu cm^{-3} hr^{-1} at $L = 3.3$, 110 amu cm^{-3} hr^{-1} at $L = 2.6$, and 248 amu cm^{-3} hr^{-1} at $L = 2.3$. *Lichtenberger et al.* [2013] used magnetometer stations from the European quasi-Meridional Magnetometer Array (EMMA) [*Lichtenberger et al.*, 2013] to measure the refilling rate using data around a storm in August 2010. They found refilling rates of 24 amu cm^{-3} hr^{-1} at $L = 3.7$, 34 amu cm^{-3} hr^{-1} at $L = 3.2$, and 45 amu cm^{-3} hr^{-1} at $L = 2.4$.

In this paper we will, in the process of improving the agreement between ground-based observations of plasmaspheric density and the DGCPM also add to the body of data points on plasmaspheric refilling and loss rates.

2. Model

The DGCPM is a single-species semi-empirical two-dimensional plasmasphere model. The modeled quantity is flux-tube content in electrons per Weber. DGCPM models the few most important processes in the plasmasphere, which are filling, depleting, and transport due to electric field drift. *Ober et al.* [1997] provides a good overview of the capabilities of the DGCPM, but we also describe the model here because we will be referring to it during the rest of this paper.

The model includes a magnetic field, an electric field, filling of plasma onto flux tubes from dayside foot points which are illuminated, and depletion of plasma from nightside foot points which are in darkness. If the magnetic field is $\vec{B}(\vec{r})$ and the electric field is $\vec{E}(\vec{r})$, defined in the magnetic equatorial plane, then the plasma continuity equation can be described by equation 1 from [*Ober et al.*, 1997].

$$\frac{D_\perp N}{Dt} = \frac{F_N + F_S}{B_i} \tag{1}$$

where $\frac{D_\perp}{Dt}$ signifies a convective derivative and N is the flux tube content in electrons per Weber. F_N and F_S are the net fluxes of plasma in the northern and southern hemispheres, respectively, and B_i is the magnetic field strength at the ionospheric footpoint of the field line, assumed to be the same at both ends of the field line in this case. This is the case for a dipole magnetic field but is not true for a more realistic magnetic field. The flux in the northern and southern hemisphere will be either filling, if the fluxtube foot point is on the dayside, or depleting if the fluxtube footpoint is on the night side. For dayside the expression is

$$F_d = \frac{n_{\text{sat}} - n}{n_{\text{sat}}} F_{\max} \tag{2}$$

where n_{sat} is the saturation number density, n is the density, and $F_{\max}$ is the maximum flux. This equation produces an exponential filling profile. On the night side exponential depletion is assumed with the expression

$$F_n = \frac{N B_i}{\tau} \tag{3}$$

where τ is the characteristic depletion time. There are thus three parameters which define the filling and depletion behavior of DGCPM, n_{sat}, $F_{\max}$, and τ. While these can be modified, the parameters used by *Ober et al.* [1997] were as follows. The saturation number density was set to

$$n_{\text{sat}} = 10^{A+B\,L} \ \text{cm}^{-3} \tag{4}$$

where $A = 3.9043$ and $B = -0.3145$, an expression which originates from the plasmasphere model of *Carpenter and Anderson* [1992], the exponent describes the average equatorial electron density variation vs. McIlwain L-value. The maximum flux is set in the *Ober et al.* [1997] model to be $F_{\max} = 2 \times 10^{12}\,\text{m}^{-2}\,\text{s}^{-1}$, and the decay-time is set to $\tau = 10\,\text{days}$.

From Equations 1-4 we can derive the following expression for the daytime flux-tube content as a function of time,

$$N(t) = N_{\text{sat}} - (N_{\text{sat}} - N_0)\, e^{-\frac{t}{\tau_d}} \tag{5}$$

where

$$\tau_d = \frac{N_{\text{sat}} B_i}{F_{\max}} \tag{6}$$

and the following expression for the night-time decay

$$N(t) = N_0 e^{-\frac{t}{\tau}} \tag{7}$$

where N_0 is the flux-tube content at the start of the refilling or decay, and t is the time since the start of the refilling or decay. In other words the daytime refilling is exponential with time-constant τ_d and the night-time decay is exponential with time-constant τ. The daytime refilling time-constant will the vary linearly with N_{sat} which is the saturation flux-tube content,

$$N_{\text{sat}} = n_{\text{sat}}\, V \tag{8}$$

The flux-tube volume is (From the Fortran code of the DGCPM model) in units of volume (m^3) per unit of magnetic flux (Wb).

$$V = \frac{4\pi\, R_E^4}{\mu_0 M}\,\frac{32}{35} L^4 \sqrt{1 - \frac{1}{L}} \left(1 + \frac{1}{2L} + \frac{3}{8L^2} + \frac{5}{16L^3}\right) \tag{9}$$

where μ_0 is the permittivity of free space, $M = 8.05 \times 10^{22}\,\text{A}\,\text{m}^2$ is the dipole moment of the Earth's magnetic field, and $R_E = 6.378 \times 10^6\,\text{m}$ is the radius of the Earth. Thus for example at $L = 3.24$ (we will return to this L-shell later) the flux-tube volume is $V\,(3.24) = 2.07 \times 10^{13}\,\text{m}^3\,\text{Wb}^{-1}$. The saturation density at that L-shell is $n_{\text{sat}}\,(3.24) = 768\,\text{cm}^{-3}$. The ionospheric magnetic field intensity is $B_i\,(3.24) = 54\,\mu\text{T}$. We arrive at a daytime refilling time-constant, $\tau_d = 5.0\,\text{d}$, or half of the decay time.

We can run the model and obtain number density estimates and compare those with observations as in Figure 1. In that figure the black curves are this model. We will discuss the red curve in a moment, and the data and data processing are discussed in the following section 3. There are two things to note. Firstly, the average value of density in the model does not match the average value of density from the data. The reason for this is simple; the model models electron number density (unit cm^{-3}) whereas the Field Line Resonance (FLR) observations produce mass density (unit $\text{amu}\,\text{cm}^{-3}$). If all ions in the plasmasphere are protons then we should expect these two measures to match. In-fact there is both He^+ and O^+ as well as other singly-ionized species in the plasmasphere which contribute to a larger mass density than that obtained from assuming only protons. The average mass per ion is often assumed to be near 2 [*Berube et al.*, 2005] and we do in-fact see, on average, roughly twice the mass density in amu per cm^3 compared to the electron number density in cm^{-3}.

The other mis-match is the slope of the diurnal variation. In the model the daily variation is much smaller than what appears to be the case from the FLR observations. This could be caused by much more rapid refilling and loss than what is modeled in DGCPM. To test this we modified the model and ran it again. That new model run is the red curve in which we set $F_{\max} = 10 \times 10^{12}\,\mathrm{m}^{-2}\,\mathrm{s}^{-1}$ and $\tau = 1\,\mathrm{d}$, increasing the outflow by a factor of 5 and reducing the decay time by a factor of 10. This change appears to improve the agreement between model and FLR-derived densities. Notice that at shell parameter L=6.14, where the trough and plumes are seen, there appears to be less effect of the change than inside the plasmasphere, e.g. at L=2.61 through L=3.62. In that regard it is worth noting that the default parameters for DGCPM were selected on the basis of comparison with observations at geostationary orbit (Ober, private communication). The diurnal variation of the modified model appears to match the observations more closely. Also, during a disturbed period, e.g. near day 43 and 44, the agreement between observations and the modified DGCPM appears to be much improved. This comparison is the motivation for the rest of this paper, to find a set of parameters which improve the agreement between this FLR-derived mass density data set and the DGCPM. The goal of this paper is not to re-write the DGCPM but rather make a tentative selection of parameters, within the existing functional form framework, which improves agreement with the observations shown in Figure 1.

3. Data

We obtained density measurements from the European quasi-Meridional Magnetometer Array (EMMA) [*Lichtenberger et al.*, 2013] established in 2012 by unifying and extending existing networks (Finnish IMAGE stations, MM100, SEGMA). EMMA consists of 25 stations (Table 1) arranged in a chain stretching from central Italy (L=1.56) to Northern Finland (L=6.42). Figure 2 shows a map of the EMMA array. Phase-gradient techniques can be used on data recorded at closely spaced meridional pairs of stations to detect the FLR frequency [*Vellante et al.*, 2014]. The equatorial mass density can be derived from the FLR frequency by solving an MHD wave equation with suitable assumptions [*Vellante and Förster*, 2006]. We solve the *Singer et al.* [1981] equation numerically along a field line determined by the International Geomagnetic Reference Field (IGRF) or some of the Tsyganenko magnetic field models (optional), while the assumed field aligned mass density distribution is simply a power-law distribution ($\rho = \rho_0(r/r_0)^{-1}$), where r is geocentric radius of a point on the field line, r_0 is the equatorial distance, ρ_0 is the mass density at r_0. Further details on the network and on density retrieval can be found at http://geofizika.canet.hu/plasmon/ and in *Lichtenberger et al.* [2013], respectively. For this paper we use observations from 8 station pairs ranging from L=2.2 to L=6.1 over a 2-month period in 2012, from September 22 until November 22. The automatically selected FLR frequencies have been manually inspected to ensure high data quality. The inversion has been executed assuming a magnetic field topology as given by the IGRF model.

4. Analysis

In this analysis we limit ourselves to determining approximate values for the following parameters: $F_{\max}$, τ, and A in the equation for n_{sat} (Equation 4). We do not examine any other parameters, nor do we modify the electric field from the default DGCPM electric field model [*Sojka et al.*, 1986].

There are some processes the DGCPM does not take into account. During storm time the ion composition changes, the average ion mass typically increases (i.e more He^+ and/or O^+ relative to H^+), especially near the plasmapause. Daytime variations near the plasmapause could be dominated by convection and not by refilling and along-the-field line depletion. Actually this happens in the cases where we see sharp dips in the time series. Density in the dips sometimes drops below a few tens of $\mathrm{amu\,cm^{-3}}$, but at least below $100\,\mathrm{amu\,cm^{-3}}$. Taking into account that here (near the plasmapause) and then (storm time) the expected average ion mass is $\gg 1$ [*Fraser et al.*, 2005], the corresponding electron density is even lower. E.g. on days 43-45 at L 3.24 and L=3.62 we observed low densities followed by much higher densities. These could be interpreted as observations outside/inside the plasmapause. These variations are produced by the variation of the convection pattern (E-field), and not by the refilling process. Whether or not the DGCPM reproduces these variations depends on how accurate the electric field model is. There is a plan to address this in a separate paper.

If we examine again Figure 1 there are days with a clear monotonic increase in plasma mass density through the daytime, and there are days which do not match this pattern very well. Generally, the days with a clear linear progression are also quiet days as measured by the planetary geomagnetic activity index Kp index. To fit the model it is necessary to select days which show only the refilling behavior and not any other dynamics that may be happening. We used two different approaches to select those days. The first, automatic, approach involved a selection criterium based on the Kp index. We selected days for further study which had a $\bar{K}p$ (average) of at most 1, and for which $\sigma\,(Kp)$ (RMS) variation around the average was at most 0.5. The motivation for the latter selection criterium was to limit the selection to days without rapid changes in Kp. 39 days satisfied $\bar{K}p \leq 1$, and of those only 17 days also satisfied $\sigma\,(Kp) \leq 0.5$. The second, manual, approach was based on a visual inspection of the data in Figure 1, looking for days with low Kp, typically less than 1, and days where the data appear to show a monotonic increase of mass density with time. The motivation for that selection was that we were looking for refilling events and wanted to exclude days where activity was evident which could disrupt this refilling. Table 2 (right) lists the days which were selected automatically based on Kp, and Table 2 (left) lists the days which were selected manually based on inspection of Figure 1.

Next we examine the daily variation of the plasma mass density in a superposed-epoch analysis approach. While most or all selected days show a increasing density with time, that slope is superimposed on top of a baseline which varies significantly. This variation in the baseline is due to storm recovery refilling in some cases, and due to longer-term variations of plasma density in other cases. For example, in Figure 1 we see some variation of plasma mass density between days 50 and 60 which is not obviously related to changes in Kp. These longer-term variations are very interesting and we can speculate on their origin, whether from changes in ionization or other process, but we will not consider any mechanisms in this paper. However, in this paper our goal is merely to remove this baseline variation such that we can examine only the daytime refilling.

The approach we take is to normalize the densities in the following way. We choose to fit a linear function,

$$\rho = \alpha + \beta\,(t - 10) \qquad (10)$$

where t is the UT time of the day in hours. 10 UT corresponds to a local time of the EMMA magnetometer stations of approximately 11-12. We use a least-absolute-deviation (LAD) [*Press et al.*, 1987] instead of a least-squares-deviation (LSD) fit to minimize the effect of outliers. A LAD fit is less sensitive to non-Gaussian-distributed outliers than a LSD fit[1]. Then we compute the average value of the offset α, $\bar{\alpha}$ and normalize each density by multiplying by the factor $\bar{\alpha}/\alpha$ to make all the fits intersect each other at 10 UT on each day. The magnitude of the correction factors, $|\bar{\alpha}/\alpha - 1|$, were small, averaging 11% for L=3.24, 2.89, 2.61, and 2.41. These are typically L-shells which present the strongest FLR signatures. At L=2.17 the correction was 47%, at L=4.09 it was 31%, and at L=6.14 it was 77%. The results are shown in Figure 3. Although FLRs can sometimes be detected on the nightside we include only dayside observations in this data set. Specifically, we excluded values which had sun zenith-angle greater then 90°. Each row of plots is for a separate L-shell as indicated in the figure, from L=6.14 in the top row to L=2.17 in the bottom row. The left column of plots contains the dates selected manually by inspection and the right column the days selected automatically by Kp. The red, green, and blue curves are the normalized daily mass density plots, shown in different colors to make it simpler to separate them visually. The grey curves are the model number densities from DGCPM for the same days. It is immediately clear that the slope with time of the measured mass density is much larger than the slope of the number density from the model. This suggests a much more rapid refilling than what is modeled by DGCPM. We also fit Equation 10 to the combined normalized data at each L-shell (i.e. the data as plotted in the panels) for each selection of days, again using a LAD fit. Those fits are the black lines. The fit parameters are shown in Table 3, including uncertainty estimates obtained with the bootstrap method. [e.g. *Press et al.*, 1992; *Efron*, 1982]

The difference between the fit parameters of the manually and automatically selected days, in Table 3, merits some discussion. Although the fits to the two data sets are somewhat different it is not obvious that the data look significantly different. For example at $L = 4.09$ the curve fit in the left column (manual) could be a reasonable fit to the data in the right column (automatic). The slopes in the data are obviously much larger than the slopes in the model, but there is also some uncertainty in those slopes. In the middle L-shell range the fits look best, but at the extreme L-shells there are clearly some bad fits. Because of the uncertainties we do not find it worthwhile at this point, with this data sample and analysis, to determine the refilling rate as a function of L-shell. Instead, in the following we will focus on one L-shell, L=3.24, where the two sample sets are very close, and where the relative uncertainty is the smallest. This is also the L-shell with the most data available. We will use the slope at L=3.24 from the manually selected samples. In terms of data quality for this study we do expect there to be a opti-

[1] The LAD fit method also has a weakness in that under some circumstances it can produce ambiguous results in that several widely different fits may have the same LAD. The reader is invited to, as an example, plot 4 points on a XY plot, two above each other at each of two X-values. Then observe than any straight curve drawn between bottom and top points will have the same smallest LAD, but only one curve will have the smallest LSD. In the end LAD and LSD and other approaches are all approximations to some optimal fit, and in this case, checking the fits visually, the dominant source of uncertainty are the data.

mal intermediate L-shell which is best. At larger L-shell there is much dynamics such that it becomes difficult to obtain days which show clear filling and loss behavior. At larger and smaller L-shells there are also fewer clear FLR signatures to process, as can be seen from the data in Figure 1.

The next step is to determine the parameters which best match the observed slopes. Although the observed slopes appear to show linear refilling whereas Equation 2 models exponential refilling we will not modify the underlying equations but instead determine the parameters which produce the best agreement with the observations. To determine the three parameters n_{sat}, $F_{\max}$, and τ, we can proceed in two steps. First we keep n_{sat} fixed at its default value and determine the values for $F_{\max}$ and τ which reproduce the linear slope best (but without necessarily matching the absolute value). Second we set τ to its newly determined value and determine the values of $F_{\max}$ and n_{sat} to minimize the difference between data and model.

In the first step we proceed as follows. (1) Run DGCPM with n_{sat} at its default value and $F_{\max}$ and τ distributed across a 2D grid. (2) Average the DGCPM runs for the manually selected days listed in Table 2 to produce an average. (3) Plot these averages and overplot the curve for L=3.24 from Table 3, multiplied by a range of values (0.01×2^N, where $N = 0, 1, \ldots, 10$). (4) Determine the value for τ which produces the best matching slope for some value of $F_{\max}$.

Figure 4 shows this slope fitting. We ran the model for a wide range of values of τ, ranging from 10 days to 0.3 days. Each panel is for a different value of τ. The dotted lines are the fitted curve from the left L=3.24 panel in Figure 3 multiplied by the factors. The solid curves in each panel are for different values of $F_{\max}$, from bottom to top 2×10^{12}, 4×10^{12}, 8×10^{12}, 16×10^{12}, 32×10^{12}, and $64 \times 10^{12}\,\mathrm{amu\,m^{-2}\,s^{-1}}$. Notice that larger values of $F_{\max}$ show evidence of rapid exponential approach to n_{sat} which is not supported by the observations. By visual inspection we determine that the optimal value for τ is likely between 0.8 d and 0.7 d (the best-fit curve is clear visually and there is enough uncertainty in the data that although a fit might yield a more precise number it would not be more accurate or more meaningful. And we fit for a value of τ in the following).

Once τ is determined all that remains is to run the model for a number of values of $F_{\max}$ and n_{sat}, and determine the best fit. In order to leave some leeway for further adjustment to τ we do this for several different values of τ, In this second set of runs we tested 6 values of τ from 1.1 days to 0.6 days, 21 values of $F_{\max}$ from 1×10^{12} to $87 \times 10^{12}\,\mathrm{amu\,m^{-2}\,s^{-1}}$, and 31 values of A in Equation 4, from 2.9 to 5.9, for a total of 3906 model runs. We then computed the difference between the models and the quiet days manually selected by inspection (the days listed in the left half of Table 2). We again normalize the data as described earlier in order to minimize the effect of long-term variations. Since the days are normalized to their average value we expect the finally fitted model to agree with the average level of the observations which seems reasonable. We computed the mean-absolute (MA) difference as well as the root-mean-square (RMS) difference. Each panel in Figure 5 corresponds to a different value of τ, and the contours show the average RMS difference in percent of the mean density at 10 UT which was fitted to be $912\,\mathrm{amu\,cm^{-3}}$. The '+' marks the minimum RMS in each panels, and the 'x' marks the minimum MA difference. Table 4 lists the minimum values. The difference between model and normalized observations is approximately 8% MA difference and 11% RMS difference with small variation across the range of τ values tested. The minimum appears to be at $\tau = 0.8\,\mathrm{d}$ or $\tau = 0.7\,\mathrm{d}$ and we selected the best fit to be for $\tau = 0.8\,\mathrm{d}$ because that is where the best fit values of A and F_{max} by the RMS and MA difference criterium appear to be most similar.

The best-fit parameters were determined to be $\tau = 0.8\,\mathrm{d}$, $F_{\mathrm{max}} = 2.3 \times 10^{13}\,\mathrm{amu\,m^{-2}\,s^{-1}}$, and $A = 4.4$, and are summarized in the Table 5 next to the original DGCPM parameters.

5. Discussion

Figure 6 repeats Figure 1 with an additional curve in blue. The blue curve represents the model using the parameters listed in Table 5. There are several important things to note in this plot. Importantly is the vertical scaling factor between the three different curves. The difference between the best-fit model (in blue) and the original DGCPM (in black) is, during quiet time, approximately a factor of two or three on average. This difference should be seen in the context of the original DGCPM representing electron number density whereas this work is fitting mass density, specifically in $\mathrm{amu\,cm^{-3}}$. The average ion mass somewhat larger than unity is consistent with a number of the previous studies we discussed [e.g. *Berube et al.*, 2005; *Takahashi et al.*, 2006], but not with the results of *Lichtenberger et al.* [2013].

The second thing to note is the much larger refilling and loss rate in the revised model compared to the original DGCPM. In the original model the daily refilling and loss is almost invisible (black traces in Figures 1 and 6). In the revised model the refilling and decay give rise to a diurnal variation of a factor of two in plasma mass density, increasing from dawn to dusk, and decreasing from dusk to dawn. This much larger increase in refilling and loss rate is also consistent with much more rapid refilling proposed by *Borovsky et al.* [2014]. Notice that while τ (night-time decay time-constant) was decreased by a factor 12.5 F_{max} (the maximum upward dayside flux) was increased by a factor of 11.5. The similarity of these two numbers is probably not a coincidence. From Equation 6 we can evaluate τ_d at $L = 3.24$. The saturation mass-density is $n_{\mathrm{sat}} = 10^{4.4-0.3145\times3.24} = 2.4 \times 10^{3}\,\mathrm{amu\,cm^{-3}}$, making $N_{\mathrm{sat}} = 4.96 \times 10^{22}\,\mathrm{amu\,Wb^{-1}}$, and $\tau_d = 1.35\,\mathrm{d}$. This should be compared with $\tau_d = 5.0\,\mathrm{d}$ we found for the parameters of the *Ober et al.* [1997] version of the model. We decreased the refilling time constant by a factor of 4.3 and we decreased the decay time-constant by a factor of 12.5. It is interesting to note that while the filling time-constant was smaller than the emptying time-constant in the *Ober et al.* [1997] version, the emptying time-constant is smaller than the filling time-constant in our revision. The result of decreasing the decay time-constant by more that the filling time-constant is that the average density falls lower compared to the saturation density in the revised model than in the original model. Smaller time-constants results in faster filling and decay through a day, as the data show. But notice also that the day-to-day refilling in this data set appears to be more rapid than that of the original model. The day-to-day refilling rate in this data set is also possibly faster than in some previously presented data sets [e.g. *Lichtenberger et al.*, 2013]. A particular day-to-day refilling time (the effective refilling time seen after storm erosion) results from a balance between the daytime refilling and the nighttime decay. Since we only considered quiet time refilling and decay in this paper and the day-to-day refilling is the result of a delicate balance between the two it may not be constrained very well. Constraining the day-to-day refilling requires considering storm-time data and is beyond the scope of this paper. It is also worth noting that we do expect the refilling and decay times to be a function of L-shell in the plasmasphere because at larger L-shells a larger volume must be filled from a similar-sized ionospheric bottleneck. This is also a topic beyond the scope of this paper which has previously been considered by *Rasmussen et al.* [1993] and *Krinberg and Tashchilin* [1982].

The third thing to note is the considerable improvement of the agreement between model and observations during storm time. We discuss each of the storm/enhanced convection periods in this paragraph as well as the next several paragraphs. We did not use any of the storm-time data to arrive at the revised model, using only the quietest days of the period, the days listed in Table 2, and we fit only for L=3.24. Nonetheless, there is a large improvement in agreement between model during storm-time as well and at other L-shells. If we first look at the storm around day 30 of Figure 6, the original DGCPM model suggests a long recovery period whereas the revised model suggests a very rapid recovery of the plasma density in the outer plasmasphere, L=3.62 and L=4.09, consistent with observations. There the modeled dip and recovery is so rapid that it does not even appear in the observations. This could be either because there is no dip, or because the dip happened while no observations were available. At L=3.24 and L=2.89 there is a small dip in the observations, and that dip is reproduced at L=3.24 by the revised model, but not well by the original model. At L=2.89 neither original nor the revised model reproduce the small decrease in plasma mass density. During the period until the next storm, around day 38 the original DGCPM is in recovery whereas the revised model, in agreement with observations, recovers rapidly. It should be noted that the recovery of plasma density is quite rapid for this data set.

At around day 38-39 there is another dip in plasma density in the models. A few data points in the middle of day 39 agree equally well with all models. At L=2.89 observations show a dip in plasma density which is not reproduced by any of the models. We proposed that this disagreement can be related either to the electric field or the magnetic field. For example the electric field model which we used, that of *Sojka et al.* [1986], may not reproduce the actual electric field for this particular storm with sufficient accuracy. Another possibility is that the tilt-free dipole magnetic field which we used is not accurate enough. At day 41 there is another period in which the measured mass density drops, but only at L=4.09, with none of the models reproducing it. That suggests also that an improved electric field model may improve agreement.

The next large event begins at the start of day 43. At L=4.09 there are two large dips in mass density in the revised model, between day 43 and day 46, and those reproduce very accurately the observations, more so than the original model. Because the double rise is so rapid we suspect it may be caused by a combination of recovery and convection of dense plasma across the magnetometer array. A similar double dip is seen at L=4.09 on days 38-39 in the revised model although there are insufficient observations for that event to show agreement. The observations at L=3.62 on day 45 show another dip in plasma density similar to the one at L=4.09 for the same time interval. That is not reproduced by any of the models. But, again we propose that this is a result of the electric field model not being an accurate representation for this event. At L=3.24 there is another small dip in plasma density which may also suggest that the electric field for the event is a somewhat larger than the one used in the model.

The remaining storm/enhanced convection events, from day 62 onward, show substantially the same features as already described; the plasma density drops rapidly and recovers rapidly, with the revised model reproducing the observations more accurately than the original model.

A fourth thing to note is that the model appears to fit the observations well at L-shells other than L=3.24. That suggests that the original parameterization of the model as a function of L-shell is quite good even if, according to the present work, the values of the parameters required some adjustment. A different parameterization, for example linear filling and exponential loss also appears to be consistent with observations, but we chose to retain the functional form of the model because it make it easier for other researchers to use the present results.

A fifth thing to note is that outside the plasmapause the densities in the revised model, in the plumes in the afternoon sector, are significantly larger in the revised model (blue curve in Figure 6) than in the original model. *Borovsky et al.* [2014] has also pointed to higher density in plumes than what is modeled by and used that as an argument for why there must be much more rapid refilling taking place. But we should also caution that the revised model at L=6.14 is extrapolated from the L=3.24 using the slope with L of the original DGCPM model.

Before we proceed with comparison to existing results it is important to distinguish between the daytime refilling, the rate at which the plasma density increases on field lines whose foot points are in sunlight, and the day-to-day refilling rate, the net refilling rate over a 24-hour period of a field line depleted, for example by a magnetic storm, taking into account the net effect of daytime filling and nighttime loss. We investigate only the daytime refilling. If we look at Figure 6 we can see from the revised model, in blue, or from the observations, black diamonds, that the density changes by approximately a factor of two on a daily basis at L=3.24, from typically $10^3\,\mathrm{amu\,cm^{-3}}$ to $2\times10^3\,\mathrm{amu\,cm^{-3}}$. This corresponds to a refilling rate at L=3.24 of approximately $80\,\mathrm{amu\,cm^{-3}\,hr^{-1}}$. We can also use the revised and original models to compute refilling rate as a function of L-shell. Since the DGCPM models exponential refilling the refilling rate will, even for steady-state conditions, vary as a function of the time since dawn such that we can obtain different refilling rates depending on where we compute it. We chose two measures of refilling rate; (a) the refilling during the first hour following dawn; (b) the hourly refilling rate averaged over the entire dayside pass of a field line. We first obtain a quiet time density map. We use October 26, 2012 at 0 UT for that. Then we compute the difference in density, for the same L-shell, from the dawn terminator to one hour of local time after the dawn terminator as well as the change in density from the dawn terminator to the dusk terminator. The difference is converted into a refilling rate with units of $\mathrm{cm^{-3}\,hr^{-1}}$. In the case of the revised model this is in units of amu, whereas in the original model it is number density. The results are shown in Figure 7. The figure plots the dawn refilling rate as a solid curve and the dayside averaged refilling rate as a dashed curve. That figure also contains, for comparison, refilling rates from several other previous works. The black curves are the refilling rates for the original model, the red curves are for the initial guess revised model, and the blue curves are for the final revised model. Notice the peak in refilling rate around L=5.7 in all three models, as well as a peak in refilling rate near L=4.4, and negative refilling rate between L=4.0 and L=4.3 for the original model. These features are all artifacts of the way in which we computed the refilling rate. We assumed azimuthal plasma drift only. This is a reasonable approximation for the most part, especially in the inner plasmasphere and outside of the plasmapause close to dawn, but it appears to cause trouble near the plasmapause as well as for the average refilling rate outside the plasmapause. It is a result of the non-azimuthal plasma drift in those cases. It is therefore unwise to give much credence to the values between about L=4 and L=6, as well as beyond L=4 for the average daily refilling rate.

The eight symbols in Figure 7 are observations obtained from previous published results. The '+' symbol is obtained from *Chi et al.* [2000]. It agrees well with our revised model, falling a little lower than the maximum dawn-side refilling rate (solid blue curve), and close to the daytime refilling rate (dashed blue curve). The diamond symbols are obtained from *Obana et al.* [2010]. The two middle L-shell observations, L=2.6, L=3.3 agree exactly with the revised model (solid and dashed blue curves), whereas the observation at L=2.3 is a little higher than the revised model and the observation at L=3.8 is smaller than the revised model. The triangle symbols are obtained from *Lichtenberger et al.* [2013]. The middle L-shell is in-fact the same station pair that we use in the present work, and the refilling rate is obtained for an event in August 2010. The larger L-shell observations, L=3.3 and L=3.7 are slight lower than the revised model but in good agreement. The lowest L-shell data points, L=2.4 is a few times smaller than the revised model and smaller than the observations in the other two papers, but still larger then the original DGCPM.

The numbers in Table 5 can also be compared with previous work. *Park* [1970] measured upward flux of electrons during refilling and obtained the value $3 \times 10^{12}\,\mathrm{m^{-2}\,s^{-1}}$. A couple of points should be made in this regard. First, the numbers listed in Table 5 are not directly comparable to Park's numbers for two reasons: (a) Park's numbers are number density and the numbers in Table 5 are mass density for the revised model, and (b) the number $F_{\max}$ in Table 5 is a maximum flux which only occurs when the flux tube is empty. Equation 2 shows the relationship between $F_{\max}$ and the actual refilling rate. The Park number is described as being in the range $3.7 < L < 3.9$. At $L = 3.62$ the density is $653\,\mathrm{amu\,cm^{-3}}$ (From Table 3, at 10 UT) whereas the saturation density is $1826\,\mathrm{amu\,cm^{-3}}$. The according to Equation 2 $F_d = 0.64 \times F_{\max} = 1.5 \times 10^{13}\,\mathrm{amu\,m^{-2}\,s^{-1}}$. This number should then be divided by the average ion mass before comparing to the value of Park. If the ion mass is 2 this evaluates to two or three times the *Park* [1970] estimate. More recent work based on FLR measurements have found as follows: $1-5\times10^{12}\,\mathrm{amu\,m^{-2}\,s^{-1}}$ for $2.3 < L < 3.8$ [*Obana et al.*, 2010], $5.7\times10^{12}\,\mathrm{amu\,m^{-2}\,s^{-1}}$ at $L = 2$ [*Chi et al.*, 2000], 1-2 $\times\, 10^{12}\,\mathrm{amu\,m^{-2}\,s^{-1}}$ at $L = 2.4$, $2 - 5 \times 10^{12}\,\mathrm{amu\,m^{-2}\,s^{-1}}$ at $L = 3.2$, $1-8\times10^{12}\,\mathrm{amu\,m^{-2}\,s^{-1}}$ at $L = 3.7$ [*Lichtenberger et al.*, 2013]. The upper end of the ranges of all these previous results appear to be consistent with our results.

A final note of caution: These data begin at the autumn equinox and run for approximately 60 days. That means that this study is biased toward equinox, and this should be taken into consideration when interpreting the results. It is possible that the refilling rates can vary with the Earth's rotation axis tilt angle because the illumination of the field line foot point is affected by this. That is a topic that we would like to explore in the future. Much more can still be done with these data sets. In this paper we fit at a single L-shell and see considerable improvement in the model.

The revised DGCPM models quiet-time mass densities, as opposed to the original DGCPM which models electron density. For those who wish to make use of our results to obtain electron density from this revision we recommend referring to the *Berube et al.* [2005], particularly their Figure 3, as well as the *Takahashi et al.* [2006] paper, particularly their Figure 8.

6. Conclusion

In this paper we made a detailed comparison of observation of mass density [*Lichtenberger et al.*, 2013] with the Dynamic Global Core Plasma Model [*Ober et al.*, 1997]. While preserving the functional form of the equations in the DGCPM we modified the DGCPM refilling and loss parameters to make it agree better with the observations. We did this for a single L-shell, L=3.24, but also found that the modified model agrees well with observations at other L-shells. We did not modify the L-shell dependence built into the DGCPM equations. The good agreement across a wide range of L-shells suggests that the original L-shell dependence built into DGCPM is good. The modification necessary to make DGCPM agree with observations was quite large. The refilling rate at geostationary orbit is about an order of magnitude larger in the revised model, and more than an order of magnitude larger in the inner plasmasphere. The loss time also had to be revised, by more than an order of magnitude, from 10 days to less than one day.

In comparison with previous work it is important to consider whether we are comparing to number density or mass density. The filling rates from previous work in Figure 7 [*Chi et al.*, 2000; *Obana et al.*, 2010; *Lichtenberger et al.*, 2013] are either in good agreement with, or smaller by up to a factor of approximately three than our estimates. When comparing with the work of *Park* [1970], which is electron flux measurements we find, when using a average ion mass of two, that our estimates are larger by a factor of two to three.

Acknowledgments. This work was supported by the European Union 7th Framework Program, 2011-2014 (under Grant Agreement No. 263218).

Funded by the Government of Hungary through an ESA contract under the PECS (Plan for European Cooperating States) and the Bolyai Scholarship of the Hungarian Academy of Sciences (B.H.). The views expressed herein can in no way be taken to reflect the official opinion of the European Space Agency.

Notes

1. FMI - Finnish Meteorological Institute, Finland
   UO - University of Oulu, Finland
   IGFPAS - Institute of Geophysics, Polish Academy of Sciences, Poland
   MFGI - Geological and Geophysical Institute of Hungary
   ZAMG - Zentralanstalt für Meteorologie und Geodynamik, Austria
   UNIVAQ - University of L'Aquila, Italy
   SANSA - South African National Space Agency, South Africa

References

Berube, D., M. B. Moldwin, S. F. Fung, and J. L. Green

(2005), A plasmaspheric mass density model and constraints on its heavy ion concentration, *Journal of Geophysical Research (Space Physics)*, *110*, A04212, doi:10.1029/2004JA010684.

Borovsky, J. E., D. T. Welling, M. F. Thomsen, and M. H. Denton (2014), Long-lived plasmaspheric drainage plumes: Where does the plasma come from?, *Journal of Geophysical Research (Space Physics)*, *119*, 6496–6520, doi:10.1002/2014JA020228.

Carpenter, D. L., and R. R. Anderson (1992), An ISEE/Whistler model of equatorial electron density in the magnetosphere, *J. Geophys. Res.,* , *97*, 1097–1108, doi:10.1029/91JA01548.

Chi, P. J., C. T. Russell, S. Musman, W. K. Peterson, G. Le, V. Angelopoulos, G. D. Reeves, M. B. Moldwin, and F. K. Chun (2000), Plasmaspheric depletion and refilling associated with the September 25, 1998 magnetic storm observed by ground magnetometers at L = 2, *Geophys. Res. Lett.,* , *27*, 633–636, doi:10.1029/1999GL010722.

Efron, B. (1982), *The Jackknife, the Bootstrap, and Other Resampling Plans*, S. I. A. M, Philadelphia.

Fraser, B., J. Horwitz, J. Slavin, Z. Dent, and I. Mann (2005), Heavy ion mass loading of the geomagnetic field near the plasmapause and ulf wave implications, *Geophysical research letters*, *32*(4).

Huba, J. D., G. Joyce, and J. Krall (2008), Three-dimensional equatorial spread F modeling, *Geophys. Res. Lett.,* , *35*, L10102, doi:10.1029/2008GL033509.

Krinberg, I. A., and A. V. Tashchilin (1982), Refilling of geomagnetic force tubes with a thermal plasma after magnetic disturbance, *Annales de Geophysique*, *38*, 25–32.

Lawrence, D. J., M. F. Thomsen, J. E. Borovsky, and D. J. McComas (1999), Measurements of early and late time plasmasphere refilling as observed from geosynchronous orbit, *J. Geophys. Res.,* , *104*, 14,691–14,704, doi:10.1029/1998JA900087.

Lichtenberger, J., M. A. Clilverd, B. Heilig, M. Vellante, J. Manninen, C. J. Rodger, A. B. Collier, A. M. Jørgensen, J. Reda, R. H. Holzworth, R. Friedel, and M. Simon-Wedlund (2013), The plasmasphere during a space weather event: first results from the PLASMON project, *Journal of Space Weather and Space Climate*, *3*(27), A23, doi:10.1051/swsc/2013045.

Maruyama, N., Y.-Y. Sun, P. G. Richards, J. Middlecoff, T.-W. Fang, T. J. Fuller-Rowell, R. A. Akmaev, J.-Y. Liu, and C. E. Valladares (2016), A new source of the midlatitude ionospheric peak density structure revealed by a new Ionosphere-Plasmasphere model, *Geophys. Res. Lett.,* , *43*, 2429–2435, doi:10.1002/2015GL067312.

Obana, Y., F. W. Menk, and I. Yoshikawa (2010), Plasma refilling rates for L = 2.3-3.8 flux tubes, *Journal of Geophysical Research (Space Physics)*, *115*, A03204, doi:10.1029/2009JA014191.

Ober, D. M., J. L. Horwitz, and D. L. Gallagher (1997), Formation of density troughs embedded in the outer plasmasphere by subauroral ion drift events, *J. Geophys. Res.,* , *102*, 14,595–14,602, doi:10.1029/97JA01046.

Park, C. G. (1970), Whistler observations of the interchange of ionization between the ionosphere and the protonosphere, *J. Geophys. Res.,* , *75*, 4249, doi:10.1029/JA075i022p04249.

Pierrard, V., and K. Stegen (2008), A three-dimensional dynamic kinetic model of the plasmasphere, *Journal of Geophysical Research (Space Physics)*, *113*, A10209, doi:10.1029/2008JA013060.

Press, W. H., B. P. Flannery, S. A. Teukolsky, W. T. Vetterling, and P. B. Kramer (1987), Numerical recipes: the art of scientific computing.

Press, W. H., S. A. Teukolsky, W. T. Vetterling, and B. P. Flannery (1992), *Numerical Recipes in C. The Arts of Scientific Computing. Second Edition*, Cambridge University Press, New York.

Rasmussen, C. E., S. M. Guiter, and S. G. Thomas (1993), A two-dimensional model of the plasmasphere - Refilling time constants, *Planet. Space Sci.*, *41*, 35–43, doi:10.1016/0032-0633(93)90015-T.

Richards, P. G., M. J. Buonsanto, B. W. Reinisch, J. Holt, J. A. Fennelly, J. L. Scali, R. H. Comfort, G. A. Germany, J. Spann, M. Brittnacher, and M.-C. Fok (2000), On the relative importance of convection and temperature to the behavior of the ionosphere in North America during January 6-12, 1997, *J. Geophys. Res.,* , *105*, 12,763–12,776, doi:10.1029/1999JA000253.

Singer, H. J., D. J. Southwood, R. J. Walker, and M. G. Kivelson (1981), Alfven wave resonances in a realistic magnetospheric magnetic field geometry, *J. Geophys. Res.,* , *86*, 4589–4596, doi:10.1029/JA086iA06p04589.

Sojka, J. J., C. E. Rasmussen, and R. W. Schunk (1986), An interplanetary magnetic field dependent model of the ionospheric convection electric field, *J. Geophys. Res.,* , *91*, 11,281–11,290, doi:10.1029/JA091iA10p11281.

Su, Y.-J., M. F. Thomsen, J. E. Borovsky, and D. J. Lawrence (2001), A comprehensive survey of plasmasphere refilling at geosynchronous orbit, *J. Geophys. Res.,* , *106*, 25,615–25,630, doi:10.1029/2000JA000441.

Takahashi, K., R. E. Denton, R. R. Anderson, and W. J. Hughes (2006), Mass density inferred from toroidal wave frequencies and its comparison to electron density, *Journal of Geophysical Research (Space Physics)*, *111*, A01201, doi:10.1029/2005JA011286.

Vellante, M., and M. Förster (2006), Inference of the magnetospheric plasma mass density from field line resonances: A test using a plasmasphere model, *Journal of Geophysical Research (Space Physics)*, *111*, A11204, doi:10.1029/2005JA011588.

Vellante, M., M. Piersanti, and E. Pietropaolo (2014), Comparison of equatorial plasma mass densities deduced from field line resonances observed at ground for dipole and IGRF models, *Journal of Geophysical Research (Space Physics)*, *119*, 2623–2633, doi:10.1002/2013JA019568.

Corresponding author: A. M. Jorgensen, Electrical Engineering Department, New Mexico Institute of Mining and Technology, 801 Leroy Place, Socorro, NM 87801, USA. (anders@nmt.edu)

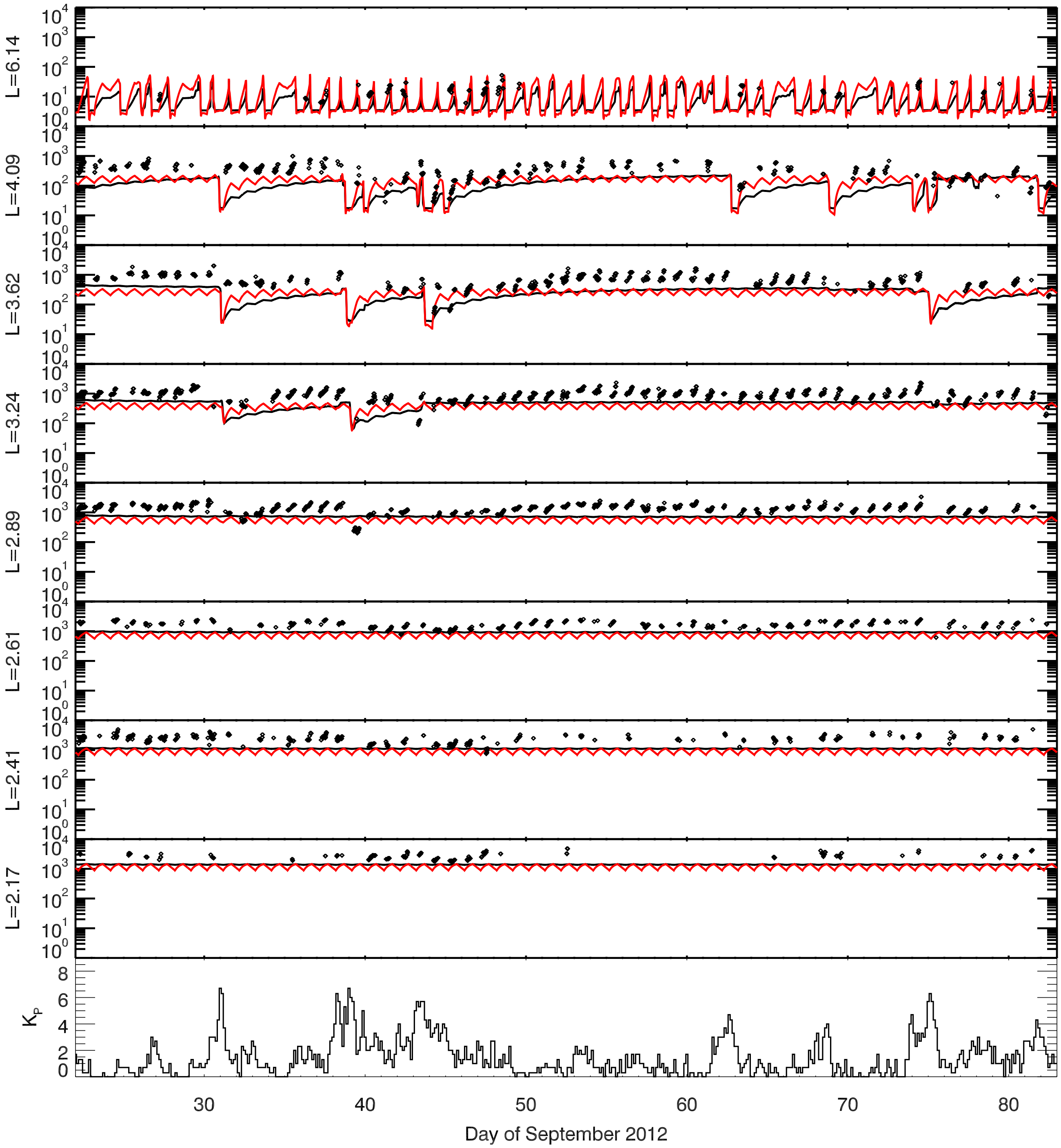

Figure 1. Comparison of the unmodified DGCPM (solid black) and a modified DGCPM (solid red), both in units of cm^{-3} with plasma mass density observations (black dots) from the EMMA array in units of amu cm^{-3}. Two things of note are (1) an average offset, a factor of 2 or more, between the unmodified DGCPM and the mass density observations. This is expected as the mass per ion is greater than 1 amu, (2) a slope in plasma mass density seen in the observations, which is not evident in the unmodified DGCPM, but which is better matched in the modified DGCPM. The bottom panel is a time-series of the planetary geomagnetic activity index Kp.

	Station	Geographic		AACGM 2012		L	1st data	Operating
Code	Name	lat.	long.	lat.	long.	shell	year	Institution[1]
KEV	Kevo	69.76	27.01	66.57	108.65	6.42	2011	FMI
MAS	Masi	69.46	23.70	66.39	105.76	6.33	2011	FMI
KIL	Kilpisjärvi	69.06	20.77	66.11	103.12	6.19	2001	FMI
IVA	Ivalo	68.56	27.29	65.34	108.04	5.83	2001	FMI
MUO	Muonio	68.02	23.53	64.92	104.63	5.65	2011	FMI
SOD	Sodankylä	67.37	26.63	64.15	106.77	5.34	2001	UO
PEL	Pello	66.90	24.08	63.75	104.40	5.19	2011	FMI
OUJ	Oulujä rvi	64.52	27.23	61.20	105.78	4.38	2011	FMI
MEK	Mekrijä rvi	62.77	30.97	59.31	108.23	3.90	2001	FMI
HAN	Hankasalmi	62.25	26.60	58.86	104.26	3.80	2011	FMI
NUR	Nurmijä rvi	60.50	24.65	57.06	101.91	3.44	2001	FMI
TAR	Tartu	58.26	26.46	54.66	102.72	3.04	2001	FMI
BRZ	Birzai	56.21	24.75	52.48	100.61	2.74	2011	IGFPAS
HLP	Hel	54.61	18.81	50.76	94.95	2.54		IGFPAS
SUW	Suwalki	54.01	23.18	50.08	98.61	2.47	2007	IGFPAS
SZC	Szczechowo	52.91	19.61	48.86	95.18	2.35	2011	IGFPAS
BEL	Belsk	51.83	20.80	47.65	95.96	2.24	2003	IGFPAS
ZAG	Zagorzyce	50.28	20.58	45.90	95.41	2.10	2011	IGFPAS
VYH	Vyhne	48.49	18.84	43.80	93.47	1.95	2011	MFGI
HRB	Hurbanovo	47.87	18.18	43.07	92.75	1.90	2000	SAS
WIC	Conrad Observatorium	47.55	15.52	43.73	90.23	1.91		ZAMG
NCK	Nagycenk	47.63	16.72	42.75	91.40	1.88	1999	UNIVAQ/MFGI
THY	Tihany	46.90	17.89	41.92	92.30	1.83	1996	MFGI
CST	Castello Tesino	46.05	11.65	40.74	86.63	1.77	2000	UNIVAQ
LOP	Lonjsko Polje	45.41	16.66	40.10	90.92	1.74	2012	MFGI
RNC	Ranchio	43.97	12.08	38.17	86.60	1.64	2001	UNIVAQ
AQU	L'Aquila	42.38	13.32	36.22	87.42	1.56	1985	UNIVAQ
TSU	Tsumeb	-19.20	17.58	-30.53	86.15	1.35		SANSA
SUT	Sutherland	-32.4	20.67	-40.92	86.40	1.84		SANSA
HER	Hermanus	-34.43	19.23	-42.33	83.83	1.93		SANSA

Table 1. List of EMMA stations. Source: http://geofizika.canet.hu/plasmon/emmast.php

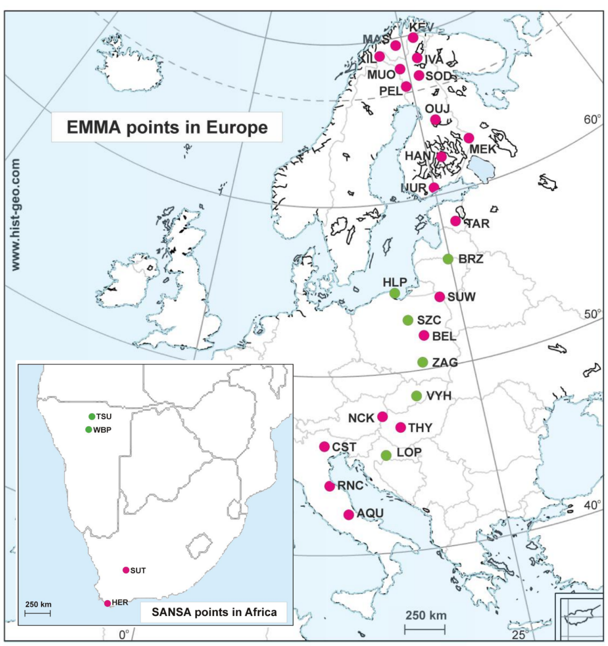

Figure 2. Map of the EMMA array stations.

Day	Date
22	2012/9/22
23	2012/9/23
34	2012/10/4
35	2012/10/5
36	2012/10/6
37	2012/10/7
48	2012/10/18
49	2012/10/19
50	2012/10/20
51	2012/10/21
52	2012/10/22
56	2012/10/26
58	2012/10/28
59	2012/10/29
60	2012/10/30
65	2012/11/4
70	2012/11/9
71	2012/11/10
73	2012/11/12

Day	Date
23	2012/9/23
24	2012/9/24
25	2012/9/25
28	2012/9/28
29	2012/9/29
34	2012/10/4
50	2012/10/20
51	2012/10/21
55	2012/10/25
57	2012/10/27
64	2012/11/3
65	2012/11/4
66	2012/11/5
69	2012/11/8
70	2012/11/9
72	2012/11/11
76	2012/11/15

Table 2. The list of quiet days selected by (left) visual inspection of Figure 1, (right) quantitative criterium based upon Kp. In both cases day number corresponds to the time-axis of Figure 1.

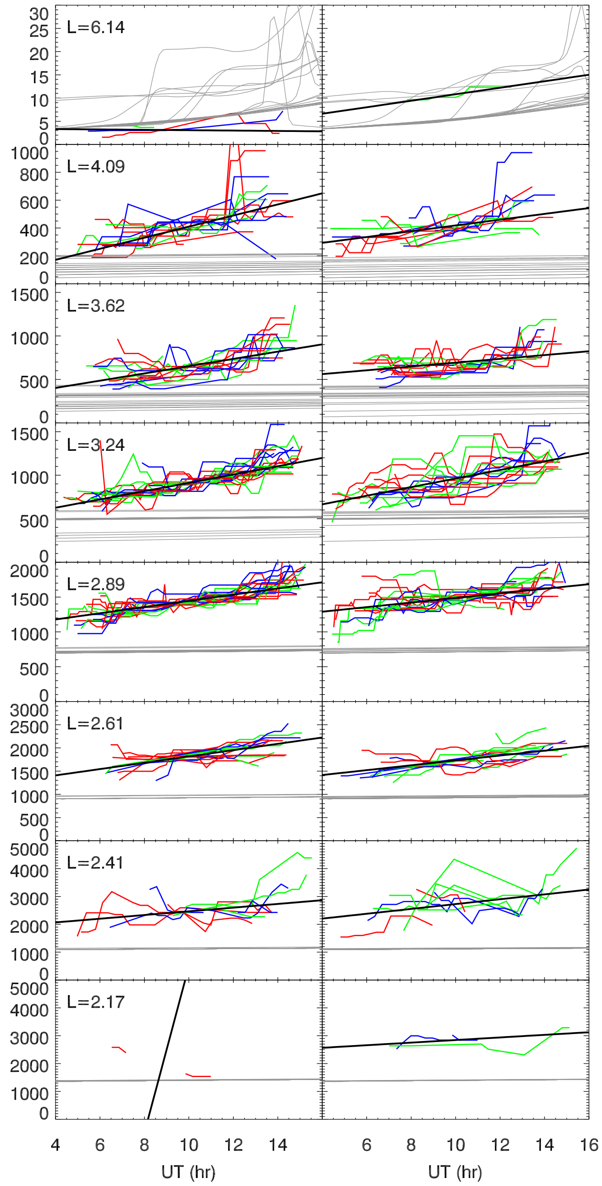

Figure 3. Mass density as a function of UT on the quiet days listed in Table 2. The left column of plots are for the days in the left column of Table 2 selected manually by inspection and the right column of plots are the days selected automatically by Kp. Each row is for a separate L-shell from $L = 6.14$ at the top to $L = 2.17$ at the bottom. The red, blue, and green colored curves are the density measurements. The gray curves are number density derived from DGCPM. Note that at L=2.17 the fits are poor because of poor normalization. However we don't make use of those fits.

	Visual				Computed			
L	α	σ_α	β	σ_β	α	σ_α	β	σ_β
6.14	3.07	0.84	-0.04	0.54	10.81	0.00	0.70	0.00
4.09	410.09	7.03	39.81	4.92	418.29	12.17	20.79	6.12
3.62	652.84	11.49	41.70	11.64	692.67	10.04	21.86	11.86
3.24	912.08	3.29	47.65	3.62	961.47	7.32	49.35	7.49
2.89	1445.23	5.11	44.50	9.73	1486.87	10.05	32.91	12.22
2.61	1815.98	21.04	68.04	26.67	1730.63	17.43	52.46	18.27
2.41	2466.17	40.85	66.38	55.23	2726.45	98.09	86.90	53.06
2.17	5493.37	5239.26	2988.70	2612.71	2844.72	23.98	46.55	39.54

Table 3. Parameters of the fitted lines in Figure 3. The first column is the L-shell. The following four columns are the parameters α and β and their estimated uncertainties for the left column of plots in Figure 3, the days selected by visual inspections, whereas the final four sets of columns are for the right column of plots, the days selected by an automated algorithm. The black lines are least-absolute-deviation (LAD) fits of Equation 10.

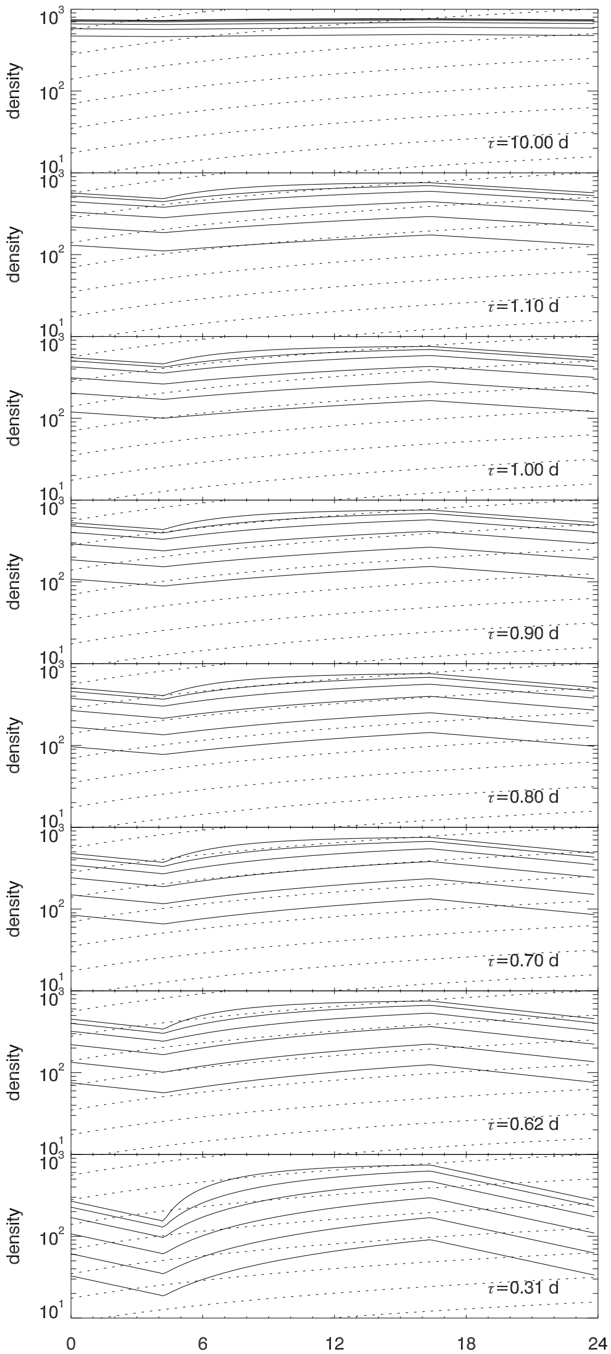

Figure 4. Comparison of the different DGCPM runs with the fitted slope of the observations. Each panel is for a different value of τ and the different DGCPM curves (solid) in each panel are for different values of $F_{\max}$. We did this calculation for a wide range of value for τ, ranging from 0.31 d to 10 d, but show only the minimum and maximum values as well as the values around 1 d. From visual inspection it appears that the 0.8 d and 0.7 d contain the best fitting curves, with the third curve from the bottom in the 0.7 d panel having a slightly too steep upward slope and the third curve from the bottom in the 0.8 d panel having a slightly too shallow slope.

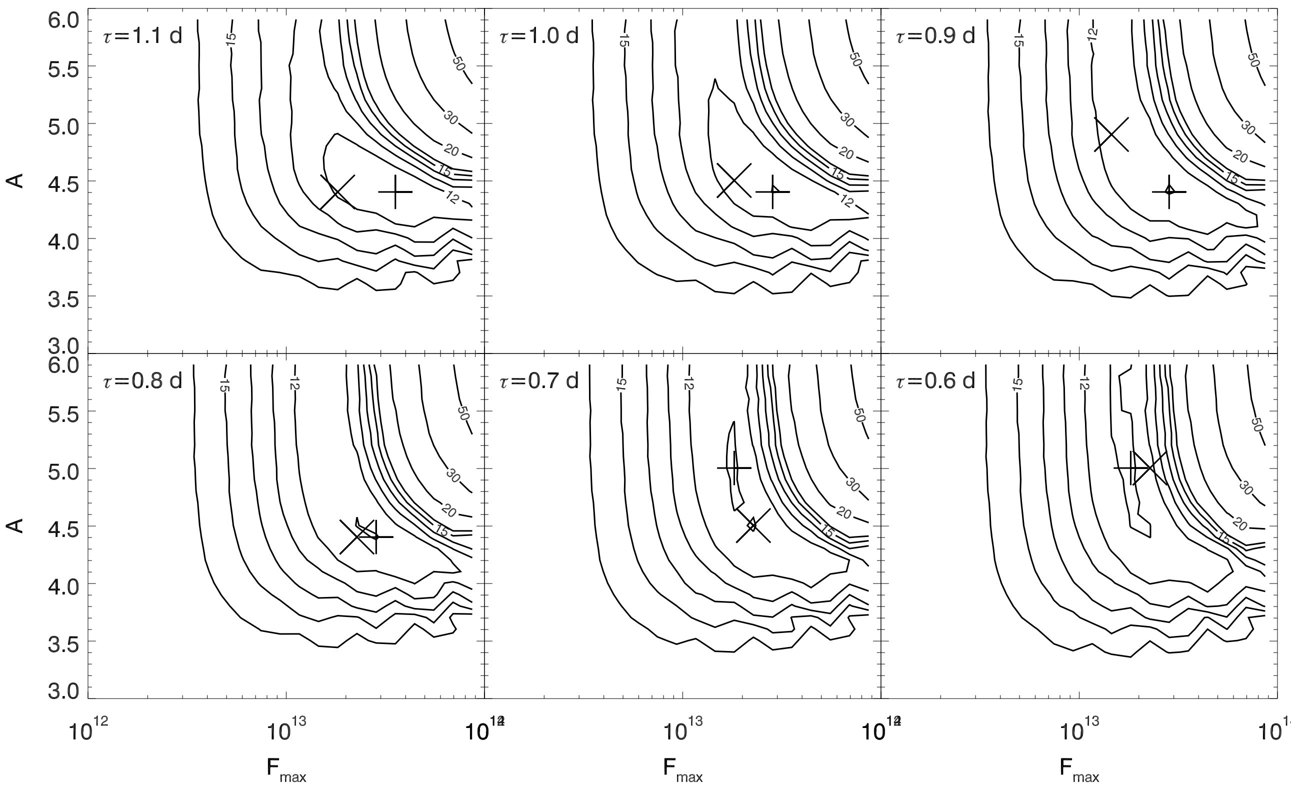

Figure 5. Contour plots of the RMS difference between model and observations normalized by the method described earlier. The differences are in percent of the mean value of the density at 10 UT (that value is 912 amu cm^{-3}). Each panel is for a different value of τ as indicated in the upper-left corner of the panel and the contour values are as a function of two order of magnitude of $F_{\max}$ on the horizontal axis and values of A corresponding to three order of magnitude of n_{sat} on the vertical axis. The '+' symbols indicate the minimum in the RMS difference whereas the 'x' symbols indicate the minimum in the absolute difference. The contours of absolute deviation are qualitatively similar and are not shown to avoid cluttering the plots. The minima are summarized in Table 4.

τ	min	$F_{\max}$	A	min	$F_{\max}$	A
1.1	8.2	1.8×10^{13}	4.4	11.0	3.6×10^{13}	4.4
1.0	7.9	1.8×10^{13}	4.5	11.0	2.8×10^{13}	4.4
0.9	7.9	1.5×10^{13}	4.9	11.0	2.8×10^{13}	4.4
0.8	7.6	2.3×10^{13}	4.4	11.0	2.8×10^{13}	4.4
0.7	7.6	2.3×10^{13}	4.5	10.9	1.8×10^{13}	5.0
0.6	8.5	2.3×10^{13}	5.0	10.8	1.8×10^{13}	5.0
Add	line	for	initial	guess		

Table 4. List of minimum absolute and RMS differences between model and data for a absolute value difference and for a RMS value difference. The minimum values are given in percent of the mean density at 10 UT (that value is 912 amu cm^{-3}). The first three sets of min, $F_{\max}$, and A are for MA difference and the second set is for RMS difference.

Parameter	Revised	Original
τ	0.8 d	10 d
$F_{\max}$	2.3×10^{13} amu m^{-2} s^{-1}	2×10^{12} m^{-2} s^{-1}
A	4.4	3.9043

Table 5. Best-fit parameters from EMMA FLR observations, left column, compared with original DGCPM parameters, right column.

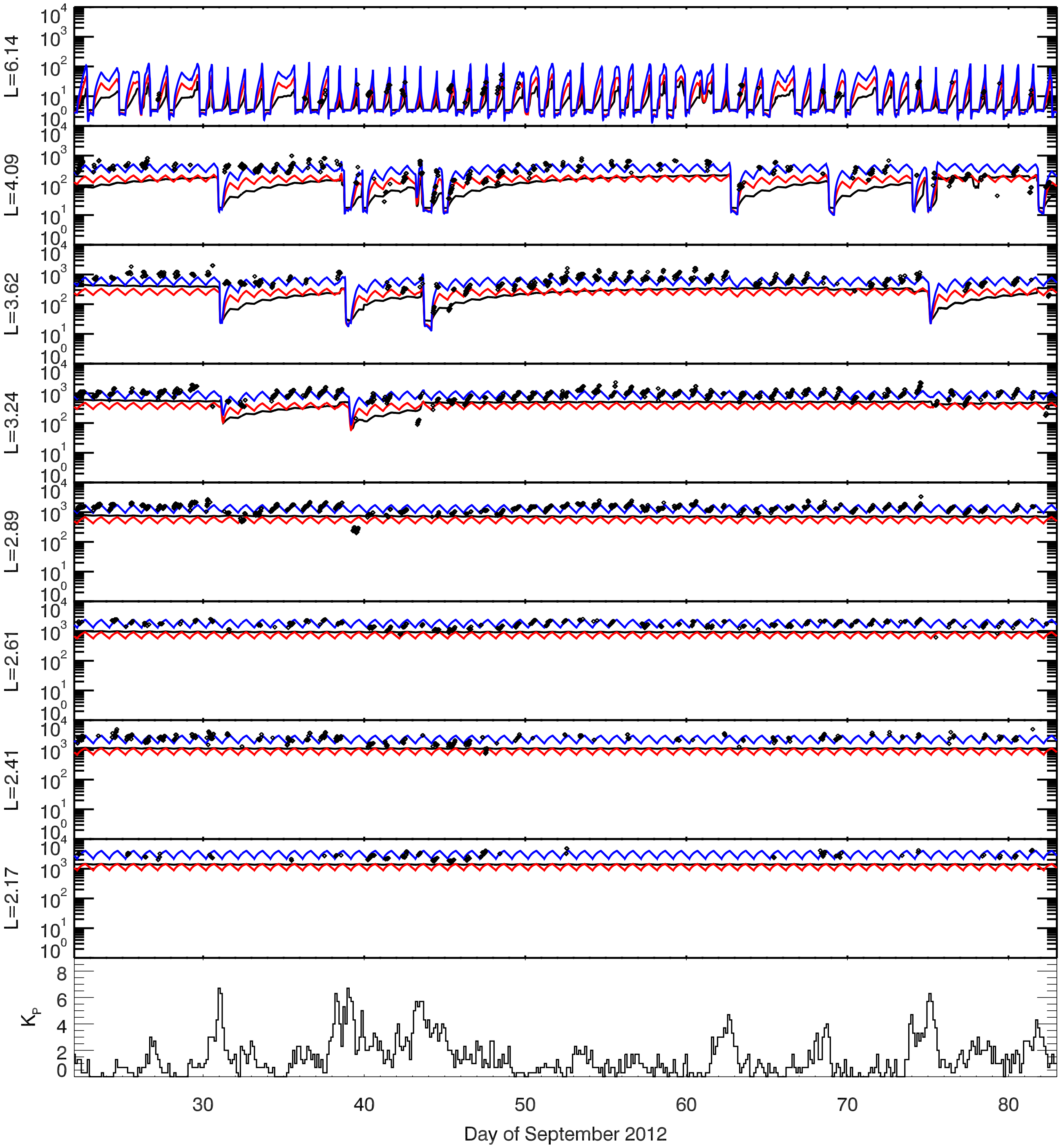

Figure 6. Final comparison of the original DGCPM model, our initial guess, and the final best-fit model. This figure is identical to Figure 1 with the addition of the best-fit model in blue.

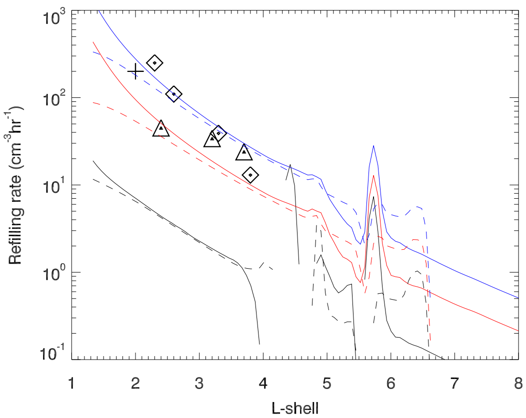

Figure 7. Refilling rates computed from model runs and compared with previous work. The solid black curve is the dawn refilling rate for the original model [*Ober et al.*, 1997] whereas the dashed black curve is the average refilling rate for the entire dayside. The solid red curve is the dawn refilling rate for the initial guess revised model, and the dashed curve is the average refilling rate for the entire dayside. The solid blue curve is the dawn refilling rate for the final revised model, and the dashed curve is the average refilling rate for the entire dayside (same colors correspond between here and Figure 6). The symbols are observations made by other groups. The '+' data point is obtained from *Chi et al.* [2000], the diamond symbols are obtained from *Obana et al.* [2010], and the triangle symbols are obtained from *Lichtenberger et al.* [2013]. The deviation from the monotonically decreasing refilling rate as a function of L-shell are artifacts of the computation method and are discussed in the text. Values between L=4 and L=6 should probably be ignored.